06

The influence of the electric field on the electrical transport properties of $(Co_{40}Fe_{40}B_{20})_x(SiO_2)_{100-x}$ nanocomposites

© A.V. Sitnikov,[1,2] Yu.E. Kalinin,[1] I.V. Babkina,[1] A.E. Nikonov,[1] D.S. Pogrebnoy,[1] A.R. Shakurov[1]

[1] Voronezh State Technical University,
394026 Voronezh, Russia
[2] National Research Center „Kurchatov Institute“,
123182 Moscow, Russia
e-mail: Aleks.shakurov@mail.ru

Received July 10, 2024
Revised November 6, 2024
Accepted November 24, 2024

The paper reveals the results of studies of the effect of electric current on the conductivity of the $(Co_{40}Fe_{40}B_{20})_x(SiO_2)_{100-x}$ nanocomposite in the composition of a metal/nanocomposite/metal capacitor-type structure. It is shown that at a high measurement current, when the reduced power exceeds 0.1 W/mm^2, the film is heated. At a power greater than 2 W/mm^2, the temperature of the sample reaches values that lead to irreversible changes in the structure of the composite. A decrease in the density of localized states in the intergranular dielectric space during thermal exposure is the determining factor in reducing the conductivity of the nanocomposite.

Keywords: Resistive switching, memristors, nanocomposite, electric properties.

DOI: 10.61011/TP.2025.01.60513.223-24

Introduction

The relevance of studying memristive structures such as metal−insulator−metal (M/I/M) that demonstrate the reversible resistive switching (RS) effect, is associated with the prospect of their use for creating matrix-type multilevel memory cells and memristor arrays simulating synapses in neuromorphic computer systems (NCS) designed to address artificial intelligence tasks [1–4].

RS in oxide-based structures is generally attributable either to the processes of electromigration of oxygen vacancies in the dielectric layer, or to the formation of channels of metal cations of the active electrode (Cu, Ag) in the dielectric layer [5–8]. As a result filamentary conductive channels (filaments) are formed (broken) in the dielectric layer. The spatial position of the formed filaments is largely random and in most cases is determined by defects in the memristor structure, which is one of the main reasons for the degradation of memristor properties in case of cyclic RS [6,7].

A possible way to solve this problem is to use nanocomposite (NC) as one of the electrodes of the M/I/M memristor structure. Conductive channels are formed from contiguous metal pellets in this case, which define the surface concentration and spatial arrangement of the filaments formed in the dielectric interlayer. Studies have shown that the bipolar resistive switching effect with a high (Roff) to low (Ron) resistance state ratio of Roff/Ron ≈ 100 which was well reproduced with the number of cycles RS $> 10^5$ can be realized in M/NC/M structures based on NC $(Co_{40}Fe_{40}B_{20})_x(LiNbO_3)_{100-x}$ [9–12]. The formation of a dielectric layer ($LiNbO_3$) with a thickness of 10−15 nm on the lower metal electrode was found in this case at the initial stage of nanocomposite growth as a result of the self-organization process [13,14].

Similar properties have been found in a number of M/NC/I/M structures, where $(Co_{40}Fe_{40}B_{20})_x(SiO_2)_{100-x}$ is NC, and the dielectric is $LiNbO_3$, $ZrYO_2$, $HfBO_2$, $TiYO_2$, etc. (the research data are prepared for publication). The memristive properties of these structures are determined by the formation of conductive filaments in the dielectric layer and the formation of a system of conductive channels in NC. On the other hand, there is almost no data about possible changes of the electrical properties of NC in the range of operating values of currents and voltages used to form RS in these memristive structures.

The purpose of this work was to identify the main mechanisms of changes of the NC electrical properties in case of exposure to electric current of various densities in a direction perpendicular to the film plane.

1. Samples and study methods

M/NC/M capacitor structures were obtained by ion beam sputtering, where films $(Co_{40}Fe_{40}B_{20})_x(SiO_2)_{100-x}$ were nanocomposites (these composites will be hereinafter referred as $(CoFeB)_x(SiO_2)_{100-x}$). Three-layer conductors Cr−Cu−Cr were used as layers of metal electrodes (M) (Fig. 1).

Three process operations of ion-beam sputtering were used to obtain the experimental samples. A multilayer Cr−Cu−Cr structure was deposited on the polycrystalline

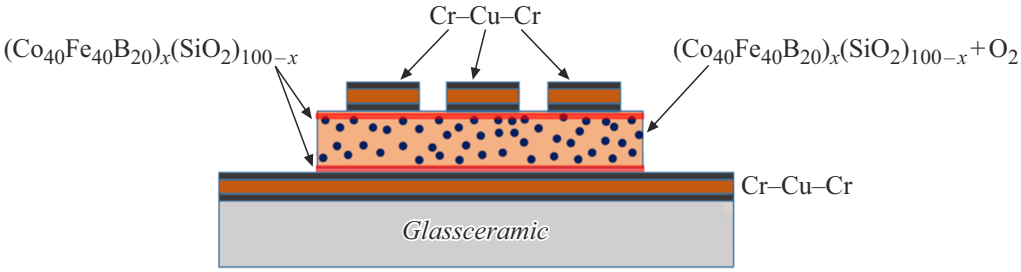

Figure 1. Topology of the experimental samples of M/NC/I/M.

glass substrates at the first stage. The choice of a multilayer configuration of the metal electrode allows, on the one hand, protecting the copper film from the impact of the natural oxidation process in the atmosphere, on the other hand, creating a buffer layer that prevents the processes of electromigration of Cu ions into the NC film, forming an electrode with a low electrical resistivity at the same time. The ion cleaning of the substrate surface was performed prior to sputtering, after which the plates were moved to the target (Cr) sputtering position, where a chromium metal film with a thickness of ~ 100 nm was sputtered for 10 min. Then, using a substrate holder with controlled rotation, the samples were moved to the target (Cu) sputtering zone, where a copper film with a thickness of ~ 1000 nm was deposited for 30 min, after which the Cr deposition operation was repeated (~ 100 nm for 10 min).

Metal-coated polycrystalline glass substrates (4 plates with a size of 60×48 mm) were arranged in a row at the second stage to obtain a deposition surface area of 240×48 mm. The substrates were covered with a shadow screen with 8 mm diameter holes arranged in 24 rows of 6 holes per row. NC film was deposited from a composite target, where 13 single crystal quartz subsamples with the size of $280 \times 80 \times 10$ mm were unevenly arranged on a $Co_{40}Fe_{40}B_{20}$ alloy wafer with a size of $80 \times 10 \times 2$ mm. This arrangement of the target allows for a smooth and continuous change of the concentration of the metal phase of the composite on the surface of the substrates, depending on the substrate–target arrangement [15,16].

Oxygen was added to the working gas atmosphere ($P_{Ar} \approx 3.9 \cdot 10^{-4}$ Torr) at a pressure of $P_{O_2} \approx 0.9 \cdot 10^{-5}$ Torr during the NC layer synthesis. A film with a thickness of ~ 250 nm was formed over the deposition time of 15 min. The composite was sputtered without any reactive gas in the first and last 20 s to form ohmic contact with metal electrodes. The metal phase concentration ranged from 14 to 39 at.% in the composite.

The top contact pads of the multilayer Cr–Cu–Cr structure were applied through a metal mask with 0.5×0.2 mm oval-shaped holes using the technology described above.

A vacuum of at least $1 \cdot 10^{-6}$ Torr was formed inside the vacuum unit prior to the start of the sputtering process. Extremely pure gases (at least 99.999% of the basic substance) were used in the sputtering process, and ion cleaning of the surface of targets and substrates was performed.

The elemental composition of NC was determined by the standard method of electron probe X-ray spectral microanalysis using energy dispersive X-ray analyzer Oxford INCA Energy 250 with JEOL JSM-6380 LV scanning electron microscope. The accuracy of identification of the composition of the samples was determined by their size, discrete location on the substrates and was ± 1 at.%.

The current-voltage curve (CVC) of M/NC/M structures and their memristive properties were measured using KEITHLEY 2450 multifunctional source-measuring device and an analytical probe station in current-limited mode. The CVC of the M/NC/M structures was measured with the bottom electrode grounded and the bias voltage U of the top electrode was scanned linearly in the sequence from $0 \rightarrow +U_{max} \rightarrow -U_{max} \rightarrow 0$ V in steps of 0.1 V. The rate of voltage change was 10 V/s.

The studied samples were successively subjected to current exposure with voltage measurement on the structure with an interval of 1 s, as shown below and in Fig. 2.

$$1 \cdot 10^{-5}\text{A} \rightarrow 5 \cdot 10^{-5}\text{A} \rightarrow 1 \cdot 10^{-4}\text{A} \rightarrow 5 \cdot 10^{-4}\text{A}$$
$$\rightarrow 1 \cdot 10^{-3}\text{A} \rightarrow 5 \cdot 10^{-3}\text{A} \rightarrow 1 \cdot 10^{-3}\text{A} \rightarrow 1 \cdot 10^{-2}\text{A}$$
$$\rightarrow 1 \cdot 10^{-3}\text{A} \rightarrow 2 \cdot 10^{-2}\text{A} \rightarrow 1 \cdot 10^{-3}\text{A} \rightarrow 4 \cdot 10^{-2}\text{A}$$
$$\rightarrow 1 \cdot 10^{-3}\text{A} \rightarrow 6 \cdot 10^{-2}\text{A} \rightarrow 1 \cdot 10^{-3}\text{A} \rightarrow 8 \cdot 10^{-2}\text{A}$$
$$\rightarrow 1 \cdot 10^{-3}\text{A} \rightarrow 1 \cdot 10^{-1}\text{A} \rightarrow 1 \cdot 10^{-3}\text{A} \rightarrow 2 \cdot 10^{-1}A$$
$$\rightarrow 1 \cdot 10^{-3}\text{A} \rightarrow 3 \cdot 10^{-1}\text{A} \rightarrow 1 \cdot 10^{-3}\text{A} \rightarrow 4 \cdot 10^{-1}\text{A}$$
$$\rightarrow 1 \cdot 10^{-3}\text{A} \rightarrow 5 \cdot 10^{-1}\text{A} \rightarrow 1 \cdot 10^{-3}\text{A} \rightarrow 6 \cdot 10^{-1}\text{A}$$
$$\rightarrow 1 \cdot 10^{-3}\text{A} \rightarrow 7 \cdot 10^{-1}\text{A} \rightarrow 1 \cdot 10^{-3}\text{A}.$$

The duration of the field exposure on the sample was 120 s with a change of the polarity of the applied voltage on the structure after 60 s. When the limiting current value on the sample exceeded $1 \cdot 10^{-3}$ A the next step was to apply a current of a higher value and again measure the electrical properties of the NC at a current equal to $1 \cdot 10^{-3}$ A. This value of the „reference“ current was chosen

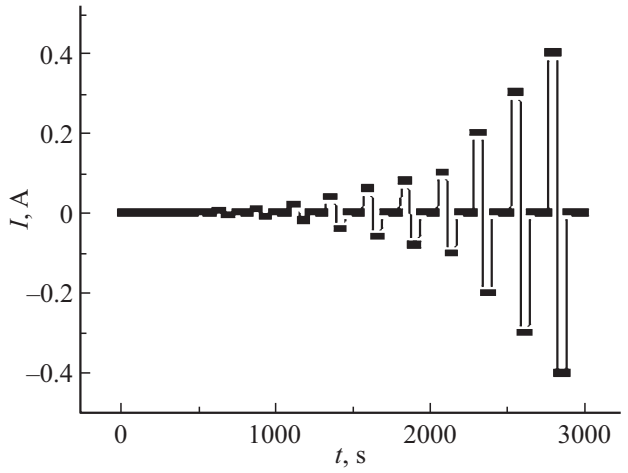

Figure 2. Time dependence of electrical impact on structure M/NC/M.

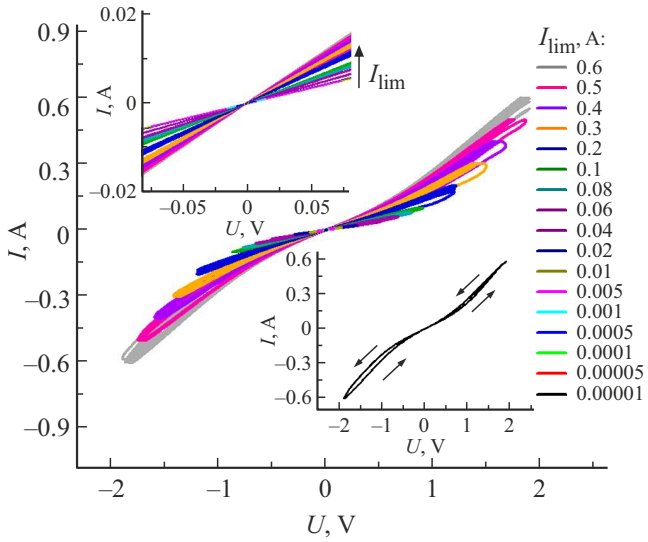

Figure 3. CVC of elements Cr/Cu/Cr/$(CoFeB)_{26.4}(SiO_2)_{73.6}$/Cr/Cu/Cr/polycrystalline glass.

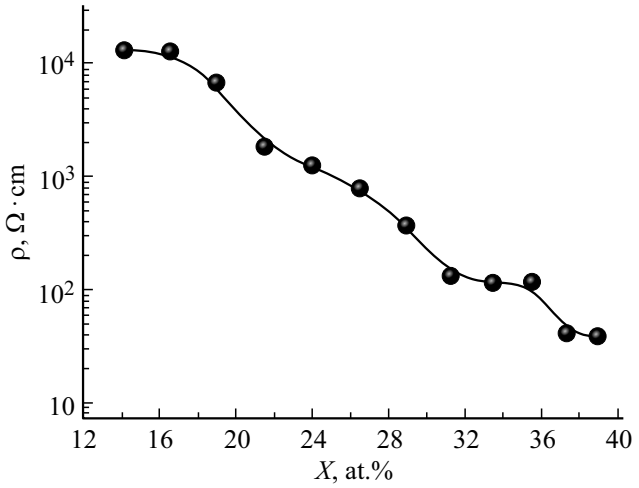

Figure 4. Concentration dependence of the electrical resistivity of a composite $(CoFeB)_x(SiO_2)_{100-x}$.

experimentally as the magnitude of the effect, which does not significantly change the resistive properties of NC. The developed algorithm of current exposure to the sample, on the one hand, makes it possible to observe the dynamics of resistive changes in the NC film under current exposure, and on the other hand, to record the degree of change of the resistance of the sample after a current load under the same measurement conditions that do not affect possible structural changes.

The electrical resistivity of the composite was measured at a limiting current of $1 \cdot 10^{-3}$ A, taking into account the resistance of the metal contacts of the structure.

2. Measurement results

A linear dependence of the CVC of the studied M/NC/M structures is observed in the entire studied range of concentration of metal phase of composite $(CoFeB)_x(SiO_2)_{100-x}$ at limiting currents of $1 \cdot 10^{-3}$ A, which suggests the presence of ohmic contact NC/M. The linearity of the CVC is upset at higher current values, and hysteresis is manifested from both the positive and negative branches of the dependence, directed towards an increase of the current value (Fig. 3). It is also possible to see a significant increase of the angle of inclination of the dependence at the origin point with an increase of the limiting current of the represented CVC.

It can be seen from the dependence $\rho(x)$ that the electrical resistivity of the composite varies by two orders of magnitude in the range of metal phase concentration from 12 to 40 at.%, which is a characteristic feature of nanostructured heterogeneous metal–isolator systems (Fig. 4) [17].

The electrical resistance of the system of Cr/Cu/Cr/$(CoFeB)_x(SiO_2)_{100-x}$/Cr/Cu/Cr/polycrystalline glass in case of application of different currents to samples in a quasi-static mode (Fig. 5) was measured to identify the causes of the change of the angle of slope of the CVC at the intersection of the origin of the characteristics of the occurrence of significant nonlinearity and hysteresis of the conductivity of the dependences $I(U)$. The measurement algorithm is described above in Sec. 1.

It can be seen that the magnitude of the electrical resistance of the composite does not change at small values of the limiting current (up to $5 \cdot 10^{-3}$ A). The value of R decreases with the increase of the measurement current at relatively higher values of I. However, this process does not affect the electrical resistance of the composite at a fixed measuring current (10^{-3} A) in a certain range of current values, which we have been taken as the „reference“ limiting current, however, this situation changes at very high limiting currents. In this case it is possible to observe the process of increasing the electrical resistance of the composite both during the exposure to current and after it.

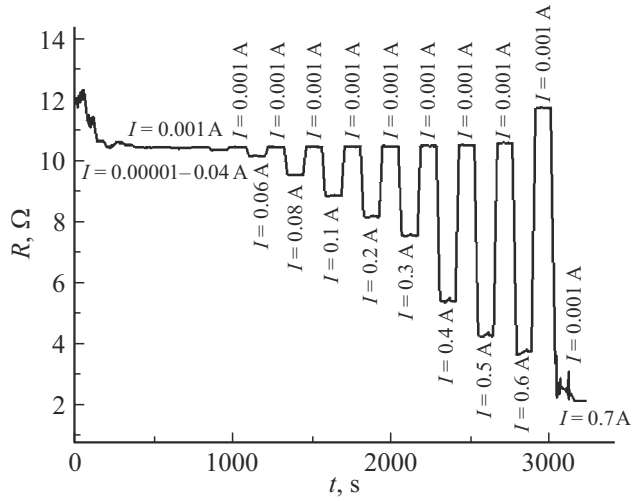

Figure 5. Time dependence of electrical resistance of composite $(CoFeB)_{23.9}(SiO_2)_{76.1}$ at different limiting currents.

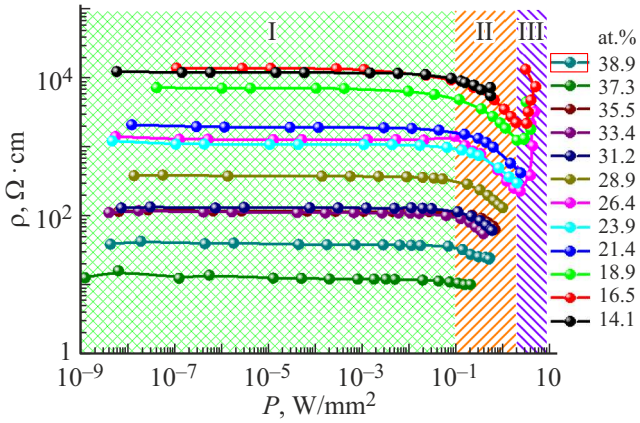

Figure 6. Dependence of the electrical resistivity of nanocomposites $(Co_{40}Fe_{40}B_{20})_x(SiO_2)_{100-x}$ in case of application of normalized power.

It can be assumed from the above characteristics that there is a process of resistive heating of the studied structure. In this case, it is convenient to analyze these dependences of the electrical resistance of the structure as a function of the reduced electrical power dissipated on the film of composite $(Co_{40}Fe_{40}B_{20})_x(SiO_2)_{100-x}$ (Fig. 6). It can be seen that the electrical resistance of the film does not change with the power of up to $P < 0.1\,W/mm^2$. The values of R decrease in the reduced power range from 0.1 to $2\,W/mm^2$, and the electric resistance sharply increases at the power of $P > 2\,W/mm^2$.

Considering that the temperature coefficient of resistance has a negative value in the entire range of the studied concentrations of the composite (the measurement data are not shown graphically, but we conducted measurements for all the studied samples), then the effect of decrease of the values of R in the area of specific power from 0.1 to $2\,W/mm^2$ becomes clear (Fig. 6, area II). A significant increase of the values of R is observed at $P > 2\,W/mm^2$ (Fig. 6, region III), which cannot be explained by a simple decrease of resistance in case of composite heating.

The electrical resistance of the sample after field exposure was measured by selecting a limiting current of 0.001 A which is located in zone I in Fig. 6 and does not cause any significant heating of the studied structure at all concentrations of the metal phase of composite $(CoFeB)_x(SiO_2)_{100-x}$. It can be seen with this representation of $\rho(P)$ that exposure of the sample for 120 s to the power from 0.1 to $2\,W/mm^2$ does not result in any irreversible changes of the electrical properties of the composite (Fig. 7, zone II) and may suggest a moderate heating of the film. It can be assumed that the increase of ρ in the region III of Fig. 6 is caused by structural changes of the studied nanocomposite, which results in the irreversible change of the electrical resistivity (Fig. 7, region III).

Several questions remain unresolved with the respect to the presented experimental results: are the structural changes caused solely by thermal heating of the composite or by the combined effects of Joule heat and the presence of an electric field? Is it possible to increase the electrical resistance in case of thermal exposure in composites at 38.9 at.% $> x >$ 28.9 at.%, where we did not reach the reduced exposure power of the sample located in zone III?

Composites $(Co_{40}Fe_{40}B_{20})_{28.9}(SiO_2)_{71.1}$ and $(Co_{40}Fe_{40}B_{20})_{38.9}(SiO_2)_{61.1}$ were thermally annealed at various temperatures for 60 min to answer these questions both in the field-free mode and with the application of a constant electric field with measuring current of 0.001 A. The current < 0.001 A does not result in any additional resistive heating of the samples. These dependencies are shown in Fig. 8. It was found that the electrical resistance of films of composite $(Co_{40}Fe_{40}B_{20})_x(SiO_2)_{100-x}$ irreversibly increases starting from temperatures of 150–200°C. Moreover, the presence of an electric field during heat treatment does not have a significant effect on this process. The heating up to a temperature of ~ 200°C does not

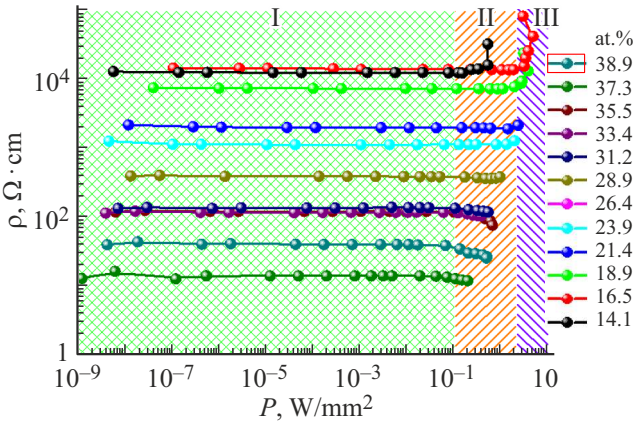

Figure 7. Dependence of the electrical resistivity of nanocomposites $(Co_{40}Fe_{40}B_{20})_x(SiO_2)_{100-x}$ after exposure to the applied normalized power measured at limiting current of $1 \cdot 10^{-3}$ A.

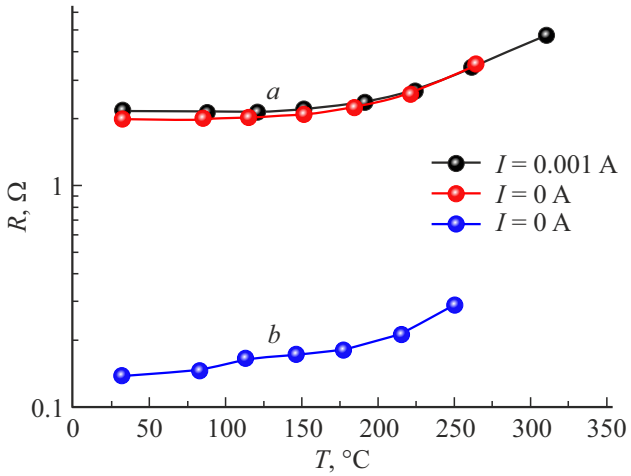

Figure 8. Dependence of electrical resistance on the temperature of annealing of composites $(Co_{40}Fe_{40}B_{20})_{28.9}(SiO_2)_{71.1}$ (*a*) and $(Co_{40}Fe_{40}B_{20})_{38.9}(SiO_2)_{61.1}$ (*b*).

result in any significant changes of the electrical properties of the studied samples.

3. Discussion of findings

Metal–isolator nanocomposites are complex nonequilibrium heterogeneous systems. The study of the structure and physical properties of composite $(CoFeB)_x(SiO_2)_{100-x}$ found that it consists of metal granules with a size of 3–6 nm, randomly embedded in a dielectric matrix [18,19]. It was also shown that not all metal atoms are concentrated in granules, but a sufficient part of them (up to $10^{22}\,cm^{-3}$) is embedded in the isolator [20,21]. The conductivity of composites up to the percolation threshold at room temperature is based either on the mechanism of hopping conductivity through localized states between the nearest neighboring states in the dielectric matrix, or on the mechanism of inelastic tunneling between granules throughout the volume of the dielectric matrix [22,23]. The atoms embedded in the dielectric phase can be denuclearized onto the surface of metal granules during thermal heating of the nanocomposite film. This should result in an increase of the volume of granules, a decrease of the electrical resistance of the conductive mesh of metal particles, and an increase of the density of conductivity channels. Our estimate of the calculated change of the particle diameter of the composite $(CoFeB)_{20}(SiO_2)_{80}$ at the concentration of dissolved particles of Co+Fe of the order $10^{22}\,cm^{-3}$ showed an increase of the size of the granules from 3 to 3.6 nm, the distance between the particles decreased from 1.7 to 1.1 nm. These are quite significant changes that can have a significant impact on the electrical properties of composite films.

The change of the concentration of defects between metal granules is another significant reason for the change of the conductivity of samples, which can act as localized states of electrons involved in electrical transfer. The concentration of these defects decreases as a result of heat exposure, which leads to an increase of the electrical resistance of the heterogeneous structure, a redistribution and a decrease of the density of conductivity channels. A visualization of this process is shown in Fig. 9.

Based on these concepts, the irreversible changes of ρ at a reduced power of more than $2\,W/mm^2$ can be correlated with resistive heating of conductive channels to temperatures of active reduction in the number of defects associated with the formation of localized electronic states in the nanocomposite dielectric matrix. This process is dominant in this temperature range, since we have not observed the effect of denuclearization of metal atoms dissolved in the dielectric phase and a decrease of the value of ρ.

The assumptions made make it possible to explain the phenomena of „breakdown“ observed in the film of nanocomposite $(CoFeB)_x(SiO_2)_{100-x}$ during the measurement of electrical resistance in the region of high values of reduced electrical power in the current fixation mode. It can be expected that a significant temperature in the conductive channel will cause a decrease of the number of localized states and, as a result, reduce the number of conductive channels involved in electrical transfer. The current is redistributed through a smaller number of conductive channels by increasing the operating voltage. The resistive heating of the conductive channels will increase, the rate of annihilation of localized states increases, and we observe the development of a classic avalanche-like process. Finally, the temperature reaches a critical value in one of the channels when a heterogeneous amorphous system crystallizes forming large CoFe crystallites with the size exceeding the film thickness ($\sim 0.1\,\mu m$), through which electrotransport occurs. The resistance of the nanocomposite film decreases, and we observe the „breakdown“ effect.

Another interesting consequence of this process is its dependence on the thermal conductivity of the substrate. It

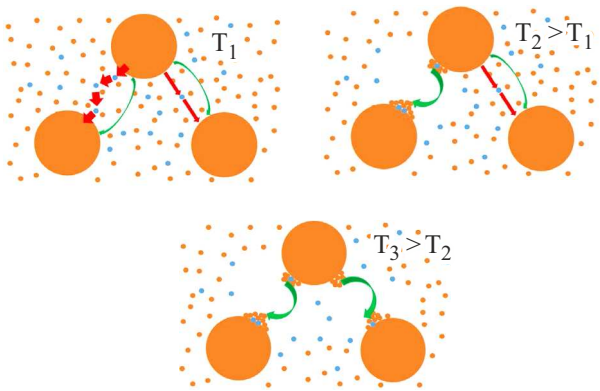

Figure 9. Model representations of the relative change of contributions to conductivity from electron tunneling from granules to granules (green arrows) and through localized states (red arrows) in case of an exposure of the nanocomposite film to heat.

can be expected that an increase of the thermal conductivity of the base of the M/NC/M structure will result in a shift of the critical specific electrical power dissipated in the film, required for the implementation of processes changing the density of localized states in the dielectric matrix towards higher values.

Conclusion

Our studies of composite conductivity $(CoFeB)_x(SiO_2)_{100-x}$ in strong electric fields have shown that at high measurement current, when the reduced power exceeds 0.1 W/mm^2, the film is heated. The sample temperature reaches values that lead to irreversible changes in the composite structure at a power greater than 2 W/mm^2. A decrease of the density of localized states in the intergranular dielectric space may be a dominant factor in the change of the conductivity value. The processes of delocalization of embedded metal atoms in the dielectric matrix, which would lead to a decrease of the electrical resistance of the sample and a change of the conductivity mechanism, have not been recorded. It is possible that these processes occur under the same thermal conditions, and the effect of decrease of the density of localized states has a more significant impact on the electrical properties of the structure.

Funding

The work has been funded by a grant from the Russian Science Foundation № 22-19-00171.

Conflict of interest

The authors declare that they have no conflict of interest.

References

[1] Z. Wang, H. Wu, G.W. Burr, C.S. Hwang, K.L. Wang, Q. Xia, J.J. Yang. Nature Rev. Mater., **5**, 173 (2020). DOI: 10.1038/s41578-019-0159-3
[2] F. Zahoor, T.Z. Azni Zulkifli, F.A. Khanday. Nanoscale Res. Lett., **15**, 90 (2020). DOI: 10.1186/s11671-020-03299-9
[3] W. Huang, X. Xia, C. Zhu, P. Steichen, W. Quan, W. Mao, J. Yang, L. Chu, X. Li. Nano-Micro Lett., **13**, 85 (2021). DOI: 10.1007/s40820-021-00618-2
[4] M. Lanza, A. Sebastian, W.D. Lu, M.L. Gallo, M.-F. Chang, D. Akinwande, F.M. Puglisi, H.N. Alshareef, M. Liu, J.B. Roldan. Science, **376**, 1066 (2022). DOI: 10.1126/science.abj9979
[5] C. Li, M. Hu, Yu. Li, H. Jiang, N. Ge, E. Montgomery, Jm. Zhang, Wh. Song, N. Davila, C. Graves, Zh. Li, J. Strachan, P. Lin, Z. Wang, M. Barnell, Q. Wu, R. Williams, J. Yang, Qf. Xia. Nature Electr., **1**, 52 (2018). DOI: 10.1038/s41928-017-0002-z
[6] D. Ielmini. Semicond. Sci. Technol, **31**, 063002 (2016). DOI: 10.1088/0268-1242/31/6/063002
[7] J.S. Lee, S. Lee, T.W. Noh. Appl. Phys. Rev., **2** (3), 031303 (2015). DOI: 10.1063/1.4929512
[8] J.J. Yang, D.B. Strukov, D.R. Stewart. Nature Nanotech., **8**, 13 (2013). DOI: 10.1038/nnano.2012.240
[9] V.V. Rylkov, S.N. Nikolaev, V.A. Demin, A.V. Emelyanov, A.V. Sitnikov, K.E. Nikiruy, V.A. Levanov, M.Yu. Presnyakov, A.N. Taldenkov, A.L. Vasiliev, K.Yu. Chernoglazov, A.S. Vedeneev, Yu.E. Kalinin, A.B. Granovsky, V.V. Tugushev, A.S. Bugaev. J. Exp. Theor. Phys., **126**, 353 (2018). DOI: 10.1134/S1063776118020152
[10] V.A. Levanov, A.V. Emelyanov, V.A. Demin, K.E. Nikirui, A.V. Sitnikov, S.N. Nikolaev, A.S. Vedeneev, Yu.E. Kalinin, V.V. Rylkov. J. Commun. Technol. Electron., **63** (5), 491 (2018). DOI: 10.1134/S1064226918050078
[11] K.E. Nikiruy, A.V. Emelyanov, V.A. Demin, V.V. Rylkov, A.V. Sitnikov, P.K. Kashkarov. Tech. Phys. Lett., **44**, 416 (2018). DOI: 10.1134/S106378501805022X
[12] V.V. Rylkov, A.V. Sitnikov, S.N. Nikolaev, V.A. Demin, A.N. Taldenkov, M.Yu. Presnyakov, A.V. Emelyanov, A.L. Vasiliev, Yu.E. Kalinin, A.S. Bugaev, V.V. Tugushev, A.B. Granovsky. JMMM, **459**, 197 (2018). DOI: 10.1016/j.jmmm.2017.11.022
[13] V.V. Rylkov, S.N. Nikolaev, K.Y. Chernoglazov, V.A. Demin, M.Y. Presnyakov, A.L. Vasiliev, V.V. Tugushev, A.B. Granovsky, A.V. Sitnikov, Y.E. Kalinin, N.S. Perov, A.S. Vedeneev. Phys. Rev. B, **95** (14), 144202 (2017). DOI: 10.1103/PhysRevB.95.144202
[14] A.V. Sitnikov, I.V. Babkina, Yu.E. Kalinin, A.E. Nikonov, M.N. Kopytin, A.R. Shakurov, O.I. Remizova, L.I. Yanchenko. ZhTF, **92** (9) (in Russian). 1382 (2022). DOI: 10.21883/JTF.2022.09.52930.94-22
[15] Yu.E. Kalinin, A.N. Remizov, A.V. Sitnikov. Phys. Solid State, **46** (11), 2146 (2004). DOI: 10.1134/1.1825563
[16] N. Domracheva, M. Caporali, E. Rentschler. *Novel Magnetic Nanostructures: Unique Properties and Applications* (Elsevier, 2018)
[17] O.V. Stognei, Yu.E. Kalinin, A.V. Sitnikov, I.V. Zolotukhin, A.V. Slyusarev. Phys. Metals Metallography, **91** (1), 21 (2001).
[18] A.V. Sitnikov. Materialovedeniye, **3**, 49 (2010).
[19] Yu.E. Kalinin, A.T. Ponomarenko, A.V. Sitnikov, O.V. Stognej. Fizika i khimiya obrabotki materialov, **5**, 14 (2001).
[20] V.V. Rylkov, A.V. Yemelyanov, S.N. Nikolaev, K.E. Nikitui, A.V. Sitnikov, E.A. Fadeev, V.A. Demin, A.B. Granovsky. ZhETF, **158** (1), 164 (2020). DOI: 10.31857/S0044451020070159
[21] A.B. Drovosekov, N.M. Kreines, D.A. Ziganurov, A.V. Sitnikov, S.N. Nikolaev, V.V. Rylkov. ZhETF, **164** (4), 650 (2023). (in Russian). DOI: 10.31857/S0044451023100176
[22] Yu.E. Kalinin, A.M. Kudrin, M.N. Piskareva, A.V. Sitnikov, A.K. Zvezdin. Perspektivnye materialy, **3**, 1 (2007) (in Russian).
[23] Yu.E. Kalinin, A.V. Sitnikov, O.V. Stogney. Vestnik Voronezhskogo gos. tekh. un-ta, **3** (11), 6 (2007) (in Russian).

Translated by A.Akhtayamov